

# Parametric investigation of nonlinear fluctuations of a dc glow discharge plasmas by using nonlinear time series analysis

Md.Nurujjaman,\* Ramesh Narayanan, and A.N.Sekar Iyengar

*Plasma Physics Division, Saha Institute of Nuclear Physics, 1/AF, Bidhannagar, Kolkata -700064, India.*

Glow discharge plasmas exhibits different kinds of nonlinear oscillations at different discharge voltages and filling pressures. The evolution of the glow discharge from its initial formation stages to the instance the discharge becomes stable, has been studied. We have invoked various nonlinear techniques like correlation dimension, Largest Lyapunov exponent etc, to study in its evolutions.

## I. INTRODUCTION

Plasma is a typical nonlinear dynamical system with many degrees of freedom, and a medium that exhibits a wide variety of nonlinear phenomena such as self oscillations, chaos, intermittency etc [1, 2, 3, 4]. Characteristics of chaos have been studied in many driven and self driven plasma systems [5, 6]. Presence of complex structures, chaos etc in the turbulent processes has also been studied in tokamaks [7, 8] and other helical devices [9] for better understanding of their role in particle transports. Recently, glow discharge of neon gas in a conventional glass tube has been analyzed for chaos, and its various roots, using power spectrum, phase space plot, correlation dimensions and Lyapunov exponents [3, 10]. This type of nonlinear system exhibits chaotic or regular behavior depending upon the parameters like discharge current, pressure etc, and transition from one state to another takes place even due to small change in the parameters. The parametric variation of the plasma properties may be modelled by few degrees of freedom [11, 12, 13, 14, 15, 16].

Motivated by the above works, we have investigated the chaotic and regular behaviors as well as their transition from one state to another with change in certain discharge parameters in argon glow discharge plasmas in a cylindrical electrode system, because such system is used in dusty plasma experiments [17] and not much investigation has been carried out in this geometry. To reveal the chaotic and regular structures in the plasma dynamics, we have deployed the well known nonlinear analysis tools like correlation dimensions, largest Lyapunov exponents and the surrogate method.

The paper has been arranged as follows: A brief description of the procedure for estimation of correlation dimension using Grassberger-Procacia algorithm [23], and the largest Lyapunov exponent using Rosenstein et al algorithm [19] which is suitable for small data length, have been presented in Section II. Section III contains the experimental setup and the results, followed by discussion and conclusion in Section IV.

---

\*Electronic address: md.nurujjaman@saha.ac.in

## II. ANALYSIS METHODS

A time series of any physical quantity measured in the laboratory is single valued. Even simultaneous multi-probe measurement of the physical quantity cannot cover all the degrees of freedom of its dynamics. So a time series may be considered as the projection of the actual dynamics on a particular degree of freedom and hence contains some incomplete information. The incomplete information can be recovered in the phase space by using delay embedding of the original time series [18]. From a time series  $(x_1, x_2, \dots, x_N)$ , where  $N$  is the total number of points, the  $m$  dimensional vector in the phase space can be constructed by delay embedding [19, 20, 21, 22]

$$X_i = [x_i, x_{i+1}, \dots, x_{i+(m-1)\tau}] \quad (1)$$

where,  $\tau$  is the fixed time lag which is usually of the order of the autocorrelation time and  $m$  is the embedding dimension. Then the reconstructed trajectory of the actual dynamics can be written as  $X = (X_1; X_2; X_3; \dots; X_M)$ , where  $M = N - (m - 1)\tau$ .

**Correlation Dimension:** Correlation dimension of a time series is defined as the dimensionality of the space occupied by the points of that time series. This dimension can be calculated from the correlation integral for the reconstructed trajectory of the time series. The correlation integral can be computed as follows [12, 19, 23, 24]

$$C(r, m) = \frac{2}{N(N-1)} \sum_{i=1}^N \sum_{j=i+1}^N \Theta(r - |X_i - X_j|) \quad (2)$$

where,  $r$  is scale length, and  $\Theta$  is the heaviside step function. Scaling of the function  $C(r, m)$  can be written as

$$C(r, m) = r^D \quad (3)$$

Correlation dimension ( $D$ ) can be defined by

$$D = \lim_{r \rightarrow 0} \lim_{N \rightarrow \infty} \frac{\partial C(r, m)}{\partial \ln r} \quad (4)$$

and for practical purpose,  $D$  can be obtained from the slope of  $\ln C(r)$  vs  $\ln r$  plot.

**Lyapunov Exponent:** Chaotic dynamical systems are sensitive to initial conditions, and exhibit an exponential divergence in the phase space. The divergence

can be quantified by an exponent which is called the Lyapunov exponent. Consider two points on two nearby trajectories in the phase space, and assume the distance between them to be  $d(0)$ . After time  $t$ , if the distance between the two trajectories becomes  $d(t)$ , then the average divergence (separation after time  $t$ ) can be written as [19]

$$d(t) = d(0)e^{\lambda_L t} \quad (5)$$

where  $\lambda_L$  is the largest Lyapunov exponent of the system. Since a practical time series is basically a scalar measurement, the largest  $\lambda_L$  can be calculated from the reconstructed trajectories in the phase space. The largest Lyapunov exponents for our data have been calculated using the algorithm proposed by Rosenstein et al since it is useful for small data length, as follows [19]:

If  $X_j$  and  $X_{j'}$  are the  $j$ -th pair of the nearest neighbor on two nearby reconstructed trajectories in the phase space, then the separation after time  $i\Delta t$ , where  $\Delta t$  is the sampling time, can written as

$$d_j(t) = d_j(0)e^{\lambda_L(i\Delta t)} \quad (6)$$

where  $d_0$  is the initial separation. Above equation can be written as

$$\ln d_j(t) = \ln d_j(0) + \lambda_L(i\Delta t) \quad (7)$$

Therefore, the largest  $\lambda_L$  can be calculated from the slope of the average line defined by

$$\langle \ln d_j(t) \rangle = \langle \ln d_j(0) \rangle + \lambda_L(i\Delta t) \quad (8)$$

where  $\langle \ln d_j(t) \rangle$  is the average divergence over all values of  $j$  at time  $t = i\Delta t$ . It is also important to note that for calculation of largest  $\lambda_L$  does not depend upon the initial separations  $\langle \ln d_j(0) \rangle$ .

### III. EXPERIMENTAL SETUP AND RESULTS

The experiments were performed in a hollow cathode dc glow discharge plasma. The schematic diagram is shown in Fig 1. A hollow S.S. tube of diameter ( $\phi$ ) 45mm was the cathode and a central rod of  $\phi$  2mm was the anode. The whole assembly was mounted inside a vacuum chamber and was pumped down to 0.001mbar using a rotary pump. The chamber was filled with argon gas up to a preset pressure, which could be controlled by a needle valve. A discharge was struck by a dc voltage which could be varied in the range of 0-1000 V. The electrostatic floating potential fluctuations have been measured using a Langmuir probe of  $\phi$  0.5mm and 2mm long, mounted in a glass tube and kept at about 12.5mm from the anode (Fig. 1) i.e. at the mid position of the anode and cathode. The plasma density was about  $10^7 \text{ cm}^{-3}$  and the electron temperature was about 3-4 eV. The corresponding elec-

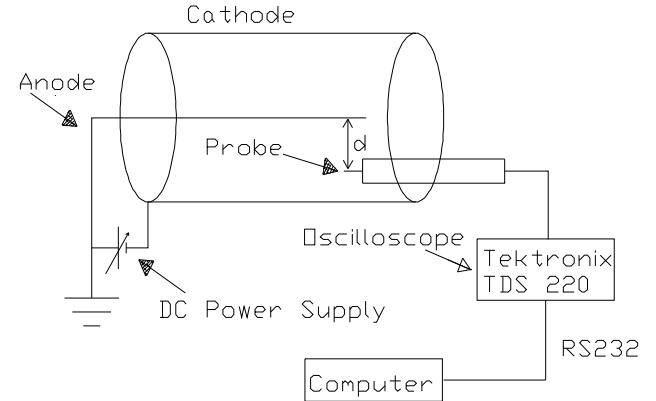


FIG. 1: Schematic diagram of the cylindrical electrode system of glow discharge plasma. The probe is placed at a distance  $d=12.5$  mm from the anode.

tron plasma frequency ( $f_{pe}$ ), and ion plasma frequency ( $f_{pi}$ ) were 28MHz, and 105kHz respectively. The data length of 2500 points was recorded at a sampling rate  $\approx 10^{-7}$  sec.

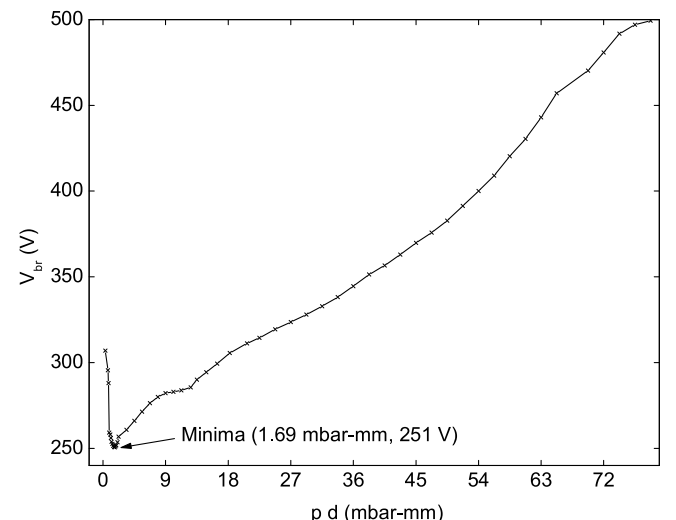


FIG. 2:  $V_{br}$  vs  $pd$  (Paschen curve) for our experimental system. The minimum occurs at (1.69 mbar-mm, 251 V)

For different filling pressures a glow is formed at different discharge voltages (DV). The breakdown voltage ( $V_{br}$ ) at which the glow is observed vs pressure x radius ( $pd$ ) has been shown in Fig 2, keeping radial distance (22.5mm) between anode and cathode fixed. The plot is almost similar to the Paschen's curve [25]. Fig 2 shows that in the low  $pd$   $V_{br}$  decreases with increase in the  $pd$ , and attains minimum at  $V_{br}=251$  V at  $pd=1.69$  mbar-mm (corresponding  $p=0.08$  mbar). Whereas, In parallel plate discharge, Paschen curve shows the minimum of  $V_{br}$  is 300 V at  $pd$  24 mbar-mm [25] for argon gas. The difference may be due to the difference in geometry of the electrode systems. It was observed that the behavior of the floating potential fluctuations for pressures less

than the Paschen minimum was different from their behavior at higher pressures. In the low pressure region (LHS of Paschen minimum) after the glow was formed, it went through two stages with increase in the DVs: at the initial stage of discharge, the system exhibited Self Organized Criticality (SOC) like behavior and after certain DV, the fluctuations changed to coherent oscillations, and with further increase in it system became turbulent and detail analysis had been presented in Ref [26]. At high pressures (RHS of the Paschen minimum), the system behaves differently with DVs, and these results have been presented here.

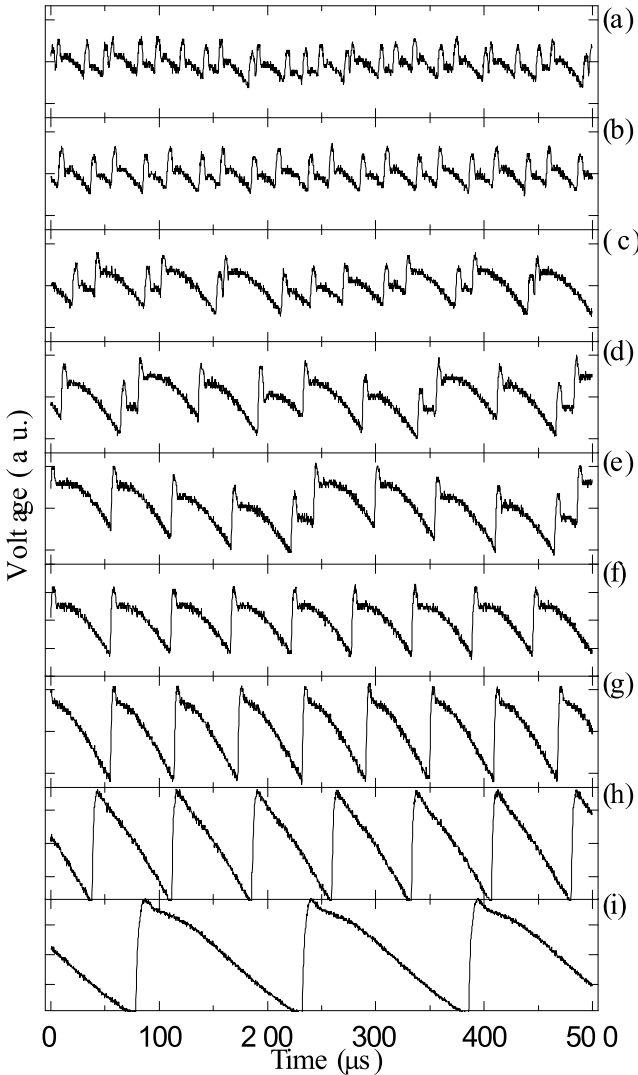


FIG. 3: Sequential change in Raw signal (normalized) at 0.89 mbar for different voltages: (a) 288 V; (b) 291 V; (c) 295 V; (d) 301 V; (e) 304 V; (f) 307 V; (g) 327 V; (h) 385 V; (i) 466 V. All y-axes range from -1 to 1.

At pressure 0.89mbar, the discharge was initiated approximately at 288V. At this particular DV, we found irregular behavior in the floating potential fluctuations as shown in Fig 3(a). But with an increase in the DVs

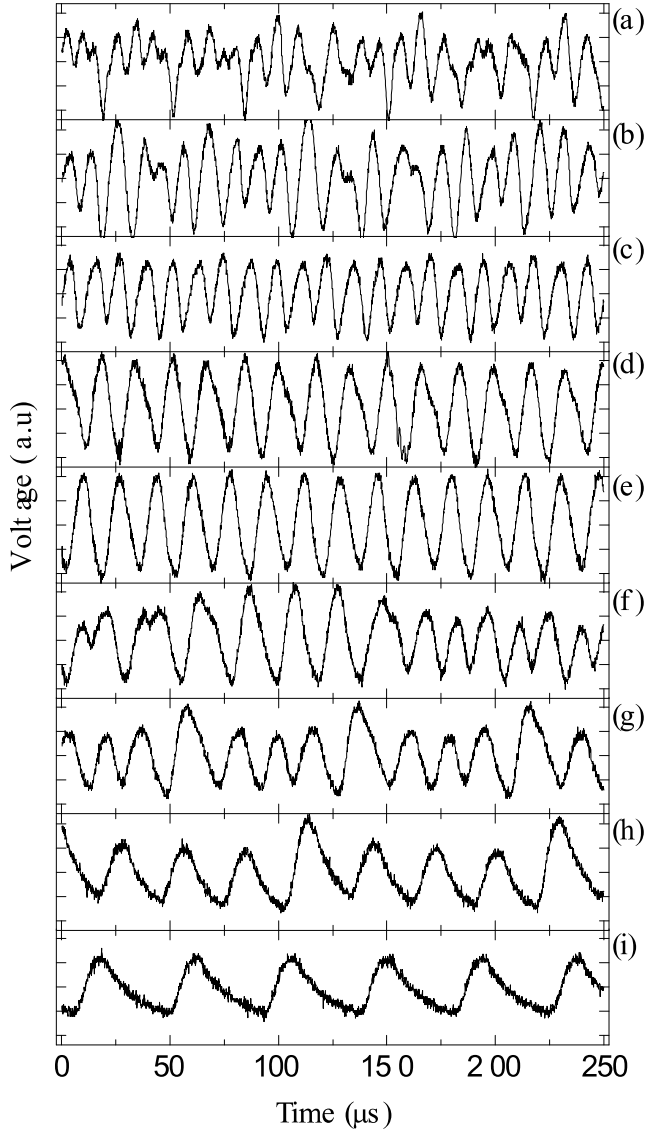


FIG. 4: Sequential change in Raw signal (normalized) at 0.95 mbar for different voltages: (a) 283 V; (b) 284 V; (c) 286 V; (d) 288 V; (e) 289 V; (f) 290 V; (g) 291 V; (h) 292 V; (i) 293 V. All y-axes range from -1 to 1.

[Figs 3(b)-3(i)], one observed the fluctuations to evolve in such a manner, so as to make a transition from an irregular to a regular behavior. It is also clear from 3, normalized signal transited to an Inverted Saw Tooth (IST) like relaxation oscillations. It is also observed that the amplitude of the oscillations increased with DVs. A complete transition to IST like relaxation oscillation observed at DV=485 V. A further increase in Voltage resulted in an increase of the time period of IST like oscillations [3(i)], culminating in a stable state at 509 V. No instabilities were observed above these voltages.

We report the experimental scan at increased pressure. We observed an interesting feature. The initial signature of a distorted IST like relaxation behavior, observed in

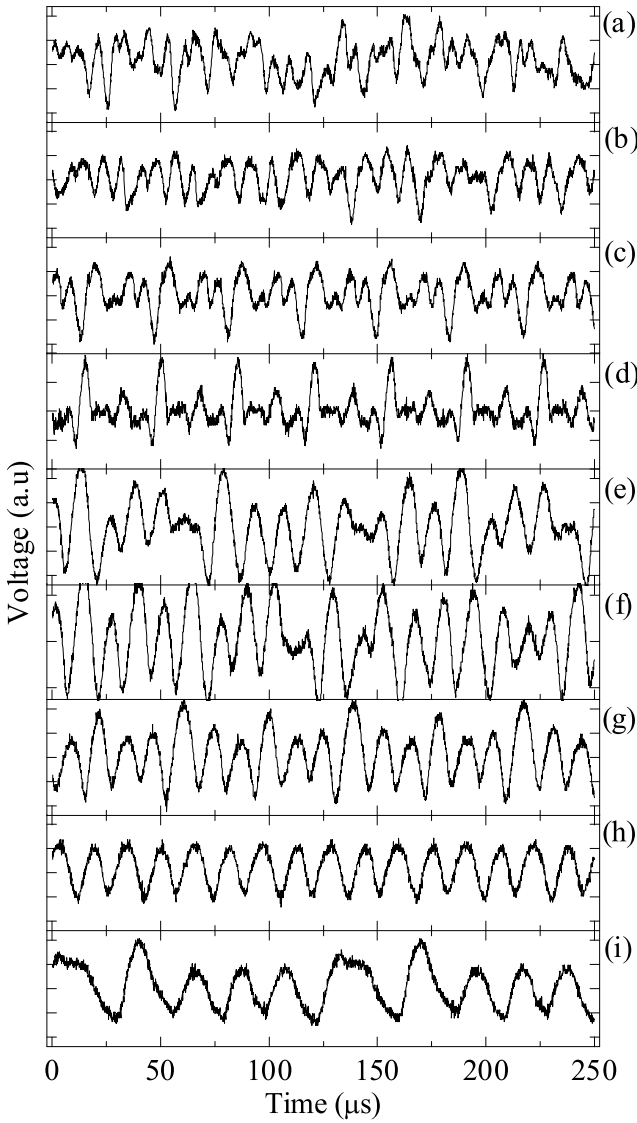


FIG. 5: Sequential change in Raw signal (normalized) at 1mbar for different voltages: (a) 293 V; (b) 296 V; (c) 298 V; (d) 299 V; (e) 300 V; (f) 305 V; (g) 308 V; (h) 310 V; (i) 312 V. All y-axes range from -1 to 1.

Fig 3, was not present. We, rather found some random fluctuations. We proceed to present the experimental results of such a voltage scan, at two higher pressures, viz 0.95mbar (Fig 4) and 1mbar (Fig 5).

At 0.95mbar we found complete irregular fluctuations in the floating potential signals, as shown in Figure 4(a) for an initial DV=283 V. With increase in the DV, the randomness in the fluctuations were reduced considerably (Figs 4(b)-4(i)), one observed that the random fluctuations slowly transited to a sinusoidal like behavior (Figs 4(c)-4(e)). However, as the voltage was increased to 290 V (4(f)), the signal became quite irregular in nature. A subsequent increase in the voltage we found onset of IST like relaxation oscillation. The scenario of such oscillations disappears completely above 293 V, wherein the

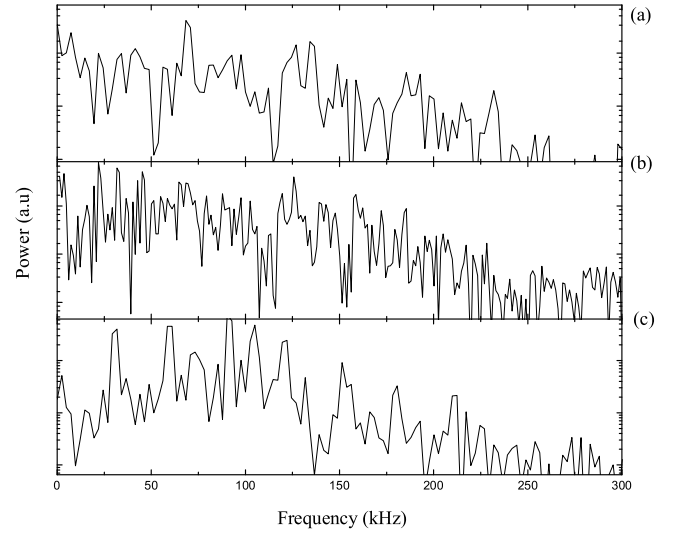


FIG. 6: Broadband power spectrum of floating potential fluctuations at initial discharge voltages at filling pressures: (a) 0.89 mbar, (b) 0.95 mbar and (c) 1 mbar. y-axis in log scale.

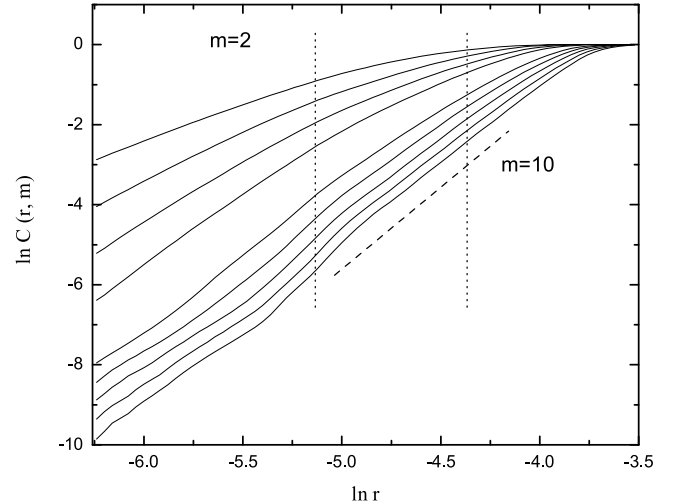


FIG. 7: Effect of embedding dimension on correlation sums. the best fitting to calculate the correlation dimension is shown by dash dot (—) line.

signal becomes stable.

In Fig5, we observed IST like relaxation oscillations at 1mbar just before attaining the stable state at 313 V, which was, however quite distorted in nature (Fig 5(i)). The window of DVs, from which a discharge was initiated to the voltage at which a stable state was attained, was much wider for 0.89mbar than 0.95mbar, and 1mbar.

A preliminary test for detecting presence of chaotic behavior in signals, is to look for a broadband behavior in FFT power spectrum. Hence we performed an FFT analysis for the signal depicted in Figs 3-5. In Fig 6, we have presented FFT plots for the three pressures 0.89, 0.95 and 1mbar at the respective DVs of 288, 283 and 293 V at which the discharge were initiated. Fig 6 clearly shows

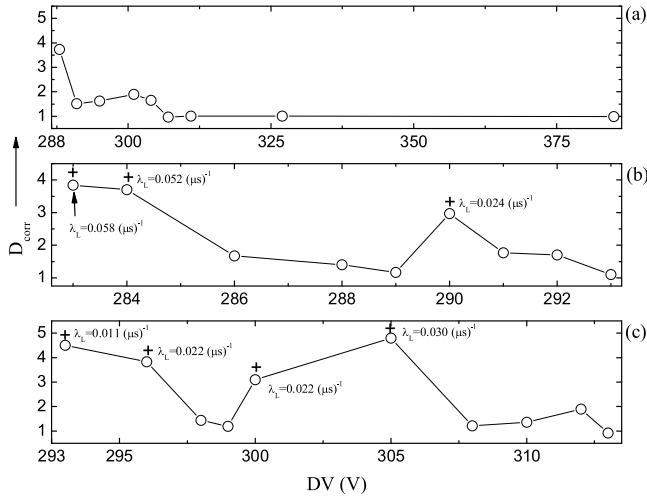


FIG. 8:  $D_{corr}$  vs discharge voltages. +Ve  $\lambda_L$  has been shown by + sign.

that the spectrum is broadband at the initial stage of the discharges. With the increase in the DVs, the broadband nature of the power spectrum is observed to decrease and distinct peaks appears. From this one can infer that the plasma floating potential does exhibit chaotic behavior at the initial phase of discharge. However since, plasma is a nonlinear medium, its properties cannot be completely characterized by only using linear techniques such as the FFT power spectrum analysis.

Keeping this in mind, we have invoked nonlinear analysis tools to estimate the correlation dimension and the largest Lyapunov exponent.

Before introducing the nonlinear analysis techniques, one should look into the stationarity of the fluctuations. This is essential because, the nonlinear analysis techniques are highly dependent on the stationarity of the signal, especially, estimation of the correlation dimension [11, 12]. The properties of the floating potential fluctuations in a dc glow discharge plasma mainly depend upon the DVs, and the filling pressures. If the set of parameters that governs the dynamics remains constant, the system output may be taken to be stationary. The controlling parameters in our system, viz. the DVs and filling pressures can be controlled as per our requirements. So we get stationary signal for a long time (probably the whole day) with a particular set of parameters and changes only with variations in these parameters.

A typical plot of  $\ln C(r, m)$  vs  $\ln r$  has been shown in Fig 7 for embedding dimensions ( $m$ ), in the range 2 to 10, from which one can calculate the correlation dimension ( $D_{corr}$ ) for DV=283 V at pressure 0.95mbar. From the same plot it is clear that the correlation sum exhibits power law behavior within a certain range of length scale ( $r$ ). Within the range shown by vertical dotted line,  $\ln C(r, m)$  vs  $\ln r$  plots are almost parallel at higher  $m$  ( $m=7-10$ ) and the corresponding best fit has been shown by — line in the same figure. The slope

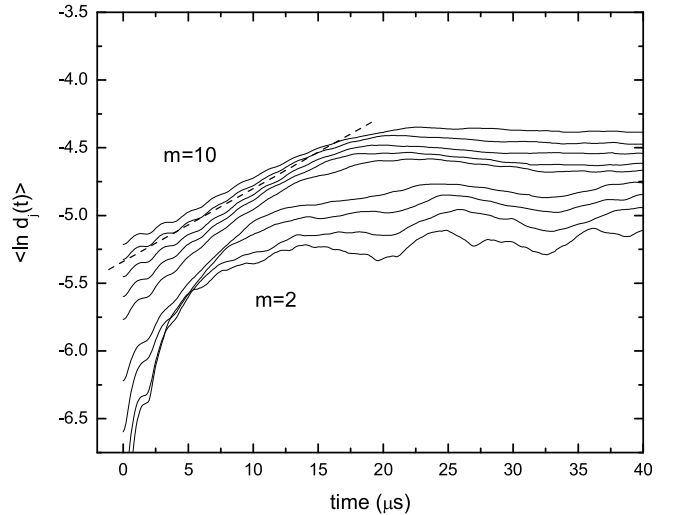


FIG. 9: Average  $\ln d_j(t)$  for different embedding dimensions. The best region for  $\lambda_L$  has been shown by dotted line.

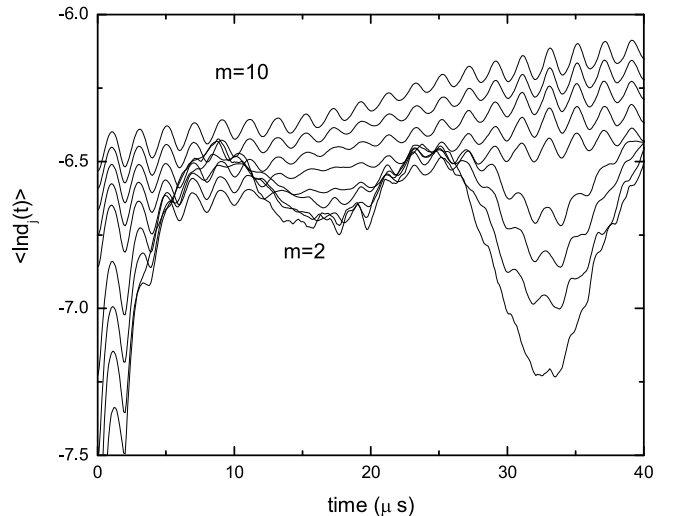


FIG. 10: For nonchaotic floating potential fluctuations we have almost flat and oscillatory divergence.

of this fit is  $D_{corr}$  of the signal at a particular  $m$ . At sufficiently high  $m$ , the value of  $D_{corr} = 3.73$ , which remains the same and this may be taken to be  $D_{corr}$  of this particular signal. The  $D_{corr}$  at the pressures 0.89, 0.95 and 1mbar for different voltages have been shown in Figs 8(a)-8(c) respectively. Fig 8(a) shows, at the initial stage of the discharge value of the  $D_{corr}$  is 3.73, and with increase in discharge voltage  $D_{corr}$  decreases uniformly and reaches unity above 305 V. In Fig 8(b) and 8(c), we observed same trend with DV. However, at pressure 0.95mbar, we get abrupt increase in  $D_{corr}$  (2.97) at DV=290 V and at 1mbar these are 3.10 and 4.80 at DVs of 300 and 305 respectively.

The complexity of the system for different DVs at different pressures can be understood by looking at the values of  $D_{corr}$ . Higher the  $D_{corr}$  more the complexity in the

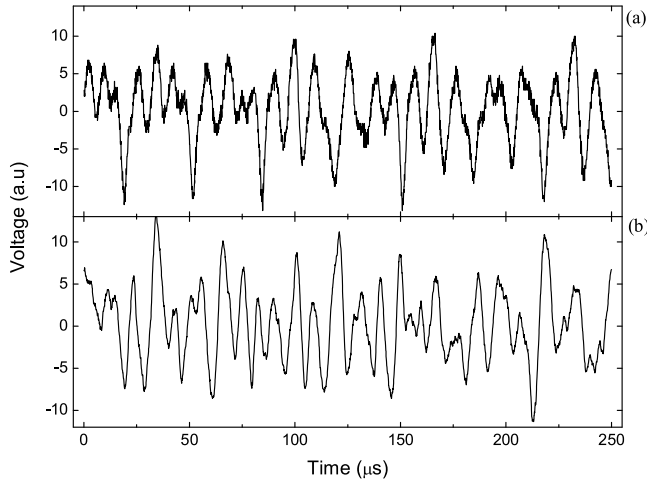


FIG. 11: Surrogate data using phase randomizing method: (a) original data; (b) surrogate data.

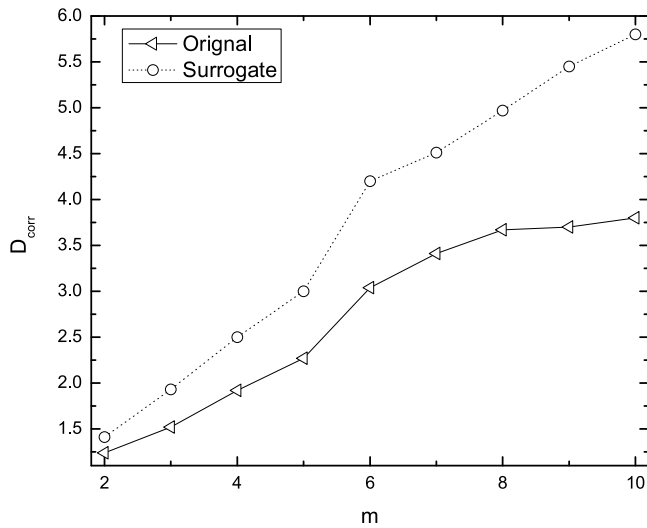


FIG. 12: Correlation dimensions vs embedding dimension for original and its surrogate data with . The correlation dimension saturates at  $D_{corr}=3.72$  for original data, whereas it increases for surrogate data.

systems [7, 8]. At the three studied pressures 0.89, 0.95 and 1 mbar, The correlation dimensions are 3.73, 3.84 and 4.5 at the initial stage of DVs. At these DVs,  $D_{corr}$  with high values may be due to the turbulent nature of the plasma, and this nature is also prominent from raw data which are visually random as seen in Figs 3(a), 4(a), and 4(a). Comparative low values in the  $D_{corr}$  at 0.89 than 0.95 and 1mbar at the initial stage of discharge may be due to presence of coherent mode along with turbulence in the first case. Sudden increase in  $D_{corr}$  at intermediate DV 290 V at pressure 0.95 mbar and at DVs 300, 305 V at pressure 1 mbar (see Figs 8(a)-(c)), indicates towards the sudden appearance of complex structures as an intermediate state in the process of regularization of plasma dynamics.

The largest  $\lambda_L$  has been calculated from the slope of the plot  $\langle \ln d_j(t) \rangle$  vs time ( $i\Delta t$ ) as shown in Fig 9 for all reconstructed phase space of dimension  $m=2$  to 10. Fig 9 shows clear scaling region for embedding dimension  $m=6$  to 10 within the time scale 0 to  $15 \mu s$ , and corresponding best fit has been shown by — line. The positive  $\lambda_L$  have been from the slope of the fitted line.

The positive  $\lambda_L$  have been shown in Figs 8(b) and (c) at pressure 0.95 mbar and 1 mbar by + sign and their values at those particular pressures where they appears. We do not get any +ve  $\lambda_L$  at pressure 0.89mbar. From Fig 8(b) it is clear that the largest  $\lambda_L$  at pressure 0.95mbar are  $0.058\mu s^{-1}$ ,  $0.052\mu s^{-1}$  and  $0.024\mu s^{-1}$  at 283, 284 and at 290 V, and at 1mbar  $0.011\mu s^{-1}$ ,  $0.022\mu s^{-1}$ ,  $0.022\mu s^{-1}$  and  $0.030\mu s^{-1}$  at DVs 293, 296, 300, and 305 V respectively. As we know +ve  $\lambda$  implies chaotic state, so at these particular DVs the system is chaotic. We may also say that the high value in  $D_{corr}$  at these particular DVs originates from chaotic dynamics. The +ve  $\lambda_L$  at intermediate DV 290 V at 0.95mbar, and at DVs 300, 305 V at 1mbar indicate sudden appearance of chaotic state between two nonchaotic state.

In order to test the nonlinearity that governs the plasma dynamics, we have applied surrogate test [27]. The surrogate data has been generated by Phase Shuffled surrogate method, in which phases are randomized by shuffling the fourier phases [11, 27, 28], and hence power spectrum (linear structure) is preserved and nonlinear structures are destroyed [28]. Using phase shuffled surrogate method, surrogate data (Figs 11(b)) from the original data (Figs 11(a)) has been generated for analysis. correlation dimensions have been estimated for both the original and surrogate data, and a  $D_{corr}$  vs  $m$  plot has been shown in Fig 12 for both the data. The  $D_{corr}$  for the original data saturates at higher  $m$ , whereas for surrogate data it increases with  $m$  which is expected, since surrogate data is random and its  $D_{corr}$  should be infinite [11]. The difference between the correlation dimensions of both types of data indicates that the fluctuations are the results of the nonlinear dynamics [11, 28].

Finally, it should be mentioned that for different pressures, we have different ranges of DVs through which the system reaches the stable state from chaotic state. For higher pressures the range of DVs through which the system attains its stable state from initial chaotic state shifts towards higher voltages. For example, at pressures 0.95 and 1 mbar the ranges of voltages are 283-293, and 293-213 V respectively.

#### IV. DISCUSSIONS AND CONCLUSIONS

The main objectives of the present study were to show how a glow dc discharge plasma system evolves at high pressure before reaching stable a state from its initial stage of discharge. For this purpose, we have investigated floating potential fluctuations as a function of Dv, and gas pressure. The result of these analyzes demonstrate

that at the initial stage of the discharge, the system exhibits chaos and with an increase in DVs complexity in the system reduces and becomes non-chaotic which have been understood from the successive decreases in  $D_{corr}$  and absence of positive  $\lambda_L$ . In the process of regularization of the dynamics, chaotic states have also been observed as a intermediate state, which occurs in such nonlinear system [10].

Though the system is nonlinear, we have applied linear tool like power spectrum which may be useful to reveal the possible source of these types of plasma instabilities. From power spectrum of the fluctuations it is observed that the upper bound of the frequencies with significant power of the instabilities are of the order of ion plasma frequencies, and lower bound is of the order of the ion transit time through the cathode sheath. Since the measurement has been performed near the cathode sheath region, So the ion dynamics near sheath and in the sheath

may be the possible source of the instabilities [4, 29].

Surface coating, and production of various nano-structures by diamond like carbon materials, nitriding processes, dust dynamics in the dusty plasmas [30, 31, 32] etc depend on the ion dynamics at the cathode sheath region. So the effects of chaos, regular behaviors and complex structures present in the plasma dynamics, on the above processes may be understood from these types of parametric studies.

### Acknowledgment

We gratefully acknowledge the use of the software for calculating largest Lyapunov exponent by M.T. Rosenstein et al. We would also like to thank S.S.Sil, D. Das, and D. Debnath for their help during the experiment.

---

[1] Ding Weixing, Huang Wie, Wang Xiaodong, and C. X. Yu, Phys. Rev. Lett. **70**, 170 (1993).

[2] W. X. Ding, H. Q. She, W. Huang, and C. X. Yu, Phys. Rev. Lett. **72**, 96 (1994).

[3] M. A. Hassouba, H.I. Al-Naggar, N.M.Al-Naggar, and C. Wilke, Phys. Plasmas **13** 073504 (2006).

[4] Md. Nurujjaman, and A.N.Sekar Iyengar, Pramana J. Phys. **67**, 299 (2006).

[5] P. Y. Cheung, and A. Y. Wong, Phys. Rev. Lett. **59**, 551 (1987).

[6] J. Qin, L. Wang, D. P. Yuan, P.Gao and B. Z. Zang, Phys. Rev. Lett. **63**, 163 (1989).

[7] H.J. Barkley, J. Andreoletti, F. gervais, J. Olivain, A. Quemeneur, and A. Truce, Plasma Phys and control fusion **30** , 217 (1998).

[8] C.P.C Prado, and N. Fiedler-Ferrari, Plasma Phys and control fusion **33** , 493 (1991).

[9] A. Komori, T. Baba, T. Morisaki, M. Kono, H. Iguchi, K. Nishimura, H. Yamada, S. Okamura, and K. Matsuaka, Phys. Rev. Lett. **73**, 660 (1994).

[10] A. Atipo, G. Bonhomme, and T. Pierre, Eur. Phys. J. D **19**, 79 (2002).

[11] Gui Dori, Shmuel Fishman, and S. A. Ben-Haim, Chaos, **10**, 257 (2000).

[12] Holger Kantz and Thomas Schreiber, *Nonlinear Time Series Analysis* (Cambridge University Press; 2nd edition, 2004).

[13] Julien Clinton Sprott, *Chaos and Time-Series Analysis* (Oxford University Press, 2004).

[14] Metin Akay, *Nonlinear Biomedical Signal Processing, Vol II: Dynamic Analysis and Modelling* (IEEE Press, 2001).

[15] H.D.I Abarbanel, R. Brown, J.J. Siderowich, and Sh. Tsimring, Rev. Mod. Phys. **65**, 1331 (1993).

[16] J.-P Eckmann, and D. Ruelle, Rev. Mod. Phys. **57**, 617 (1985).

[17] J. Pramanik, G. Prasad, A. Sen, and P. K. Kaw, Phys. Rev. Lett. **88**, 175001 (2002).

[18] T. Schreiber, Phys. Reports **308**, 1-64 (1999).

[19] Michael T. Rosenstein, James J. Collins, and carlo J. De Luca, Physica D **65**, 117 (1993).

[20] Kevin Judd, and Alistar Mees, Physica D **82**, 426 (1995).

[21] N. H. Packard, J.P Cruchfield, J.D. Farmer, and R.S. Shaw, Phys. Rev. Lett., **45** , 712 (1980).

[22] F. Takens, Detecting strange attractors in turbulence, Lecture notes in mathematics, Vol. 898 (Springer, Berlin, 1981, page 366).

[23] Grassberger P., and Procacia I, Phys. Rev. Lett. **50**, 346 (1983).

[24] Grassberger P., and Procacia I, Phys. Rev. A **28**, 2591 (1983).

[25] Von Engel, A.: *Electric plasmas : their nature and uses*, (Taylor & Francis 1983).

[26] Md. Nurujjaman, and A.N.Sekar Iyengar, Phys Letts A (2006); doi:10.1016/j.physleta.2006.09.005.

[27] James Theiler, Stephen Eubank, André Longtin, and Bryan Galdrikian, Physica D **58**, 77 (1992).

[28] T. Nakamura, and M. Small, International Journal of Bifurcations and Chaos **16**, (2006), in press.

[29] D. Arbel, Z. Bar-Lev, J. Felsteiner, A. Rosenberg, and Ya. Z. Slutsker, Phys. Rev. Lett. **71**, 2919 (1993).

[30] Ellen Meeksa, and Pauline Hob, Thin Solid Films **365** 334 (2000).

[31] A. Salifu, G. Zhang, and Edward A. Evans, Thin Solid Films **418**, 151 (2002).

[32] B. P. Pandey, G. S. Lakhina, and Vinod Krishan, Phys. Rev. E **60**, 7412 (1999).